



Optimal discharge placement in plasma-assisted combustion of a methane jet in cross flow

Wookyung Kim, Hyungrok Do, M. Godfrey Mungal, Mark A. Cappelli *

Mechanical Engineering Department, Stanford University, Bldg. 520, Duena Street, Stanford, CA 94305-3032, USA

Received 23 June 2007; received in revised form 2 November 2007; accepted 15 November 2007

Available online 4 March 2008

Abstract

Repetitively pulsed, nonequilibrium plasma discharges are studied for their ability to ignite and stabilize methane jet flames in cross flow air. The placement of the discharge is surveyed to optimize the flame duty cycle (stability). We find that flame ignition is not achieved when the discharge is located in the potential core region of the fuel jet or on the windward side of the most upstream part of the near field of the jet. A low (but nonzero) duty cycle is seen when the discharge is placed on the leeward side of the upstream near-field region. A high duty cycle (up to unity) is seen for discharge placement on both the leeward and windward sides of the downstream part of the near field. These results confirm that the effectiveness of the nonequilibrium discharge in stabilizing this flame depends on its placement in the complex scalar and velocity field. The mixture fraction at the discharge placement is characterized by plasma-induced breakdown spectroscopy (PIBS). The ratio of emission intensity of the CN band at 388 nm to the N₂ band at 337 nm is used to map the local equivalence ratio in the flow. We find that the methane mixture fraction at optimal discharge placements is lower than that where the flame resides in non-discharge-stabilized diffusion flames and is equal to that found in plasma-assisted methane jets in coflow air. Planar laser-induced fluorescence (PLIF) imaging of CH radicals is carried out to qualitatively understand the structure of the ignition flame kernel. The plasma discharge and flame base are spatially separated, suggesting that the discharge is a steady supplier of reactive species but not an instantaneous flame ignition source.

© 2008 The Combustion Institute. Published by Elsevier Inc. All rights reserved.

Keywords: Plasma-assisted combustion; Nonequilibrium discharge; Jet in cross flow

1. Introduction

Recent increased demand for high-power/low-emission combustion and the trend toward the utilization of low-grade fuels has caused renewed attention to the burning of hydrocarbons. High power combustion requires a high throughput of fuel and oxidizer,

usually implying high flow speeds, which in turn diminishes the stability of both diffusion and premixed flames. To reduce harmful emissions such as NO_x, flames are often highly diluted, further resulting in a negative effect on flame stability. Also, with greenhouse gas concerns, current efforts to expand the available fuel base leads to the consideration of biomass, such as tree prunings, plant waste, and non-recyclable paper, as alternative fuel sources. The low heating value and high concentration of impurities in biomass fuels also decreases flame stability.

* Corresponding author. Fax: +1 (650) 723 1748.

E-mail address: cap@stanford.edu (M.A. Cappelli).

Various stabilization methods have been implemented for both diffusion and premixed flames. These include pilot flames, recirculation flow via bluff bodies, swirl, electric fields, and plasmas. To attach a hydrocarbon flame to a burner lip, Han and Mungal [1] and Muñiz and Mungal [2], used a hydrogen pilot flame in a jet diffusion flame in coflow. Carter et al. [3] used a pure oxygen coflow surrounding a laboratory-scale jet diffusion flame. Prakash et al. [4] increased premixed flame stability by controlling the flow rate split between a bypass line and the main fuel line. Tachibana et al. [5] investigated the effect of secondary fuel injection location on premixed combustion instability. Typical examples of bluff body and swirl stabilization can be found in Schefer et al. [6], Yegian and Cheng [7], and Archer and Gupta [8]. However, these methods have an intrinsic limit in that the main energy transfer occurs predominantly in the form of thermal energy, which implies that a portion of it is lost while local thermal equilibrium is established. Furthermore, in the case of bluff-body and swirl-stabilization approaches, increasing entrainment of high-temperature burned gas into the fresh reacting jet by recirculation, along with longer residence times of the flow in the reaction region by swirling motions, may also lead to significant increase in the formation of nitric oxide (NO).

Interestingly, there have also been efforts to improve flame stability by controlling flow convection in the flame reaction zone with electric fields. In particular, Calcote [9] and Calcote and Pease [10] observed flame deflection and blowout limit extension of a Bunsen burner exposed to a direct current (dc) electric field. They reported that the flow rate of the Bunsen burner at the blowout limit can be increased up to 100% by use of an electric field. They suggested that these effects are caused by an “ionic wind” between the applied electric field and the “chemionized” species in the flame reaction zone. A further extension of the flame stability limit was observed by Calcote and Berman [11], with the blowout limit (i.e., flow rate) of a premixed methane/air flame increased by a factor of ~ 4 , when a dc field was applied. Investigations of blowout limit and burning velocity increases seen under alternating current (ac) were also reported by Polanyi and Markstein [12], Tewari and Wilson [13] and Maclatchy et al. [14]. However, the improvements to the blowout limit and burning velocity with ac electric fields have been marginal in comparison to those with dc fields. A comprehensive review of those observations is described by Lawton and Weinberg [15] and Fialkov [16]. Very recently, Won et al. [17] applied an ac electric field to a laminar lifted propane flame in air coflow. They observed that the propagation speed of the propane edge flame increased by $\sim 60\%$. Prior work regarding the inter-

action between flames and plasma discharges can be found in the papers of Weinberg et al. [18], Carleton et al. [19], and Lee and Weinberg [20]. They used near-equilibrium plasma jets to increase flame speed and expand the flammability limit of premixed flames. Even though the flame stability increase due to the presence of electric fields is quite promising, as shown, it is noteworthy that most of the previous studies were carried out under laminar flame conditions, which implies that a more compelling (but still non-thermal) means of stabilization enhancement may be required for turbulent flames.

Recent activity to investigate novel flame stabilization approaches has included the use of nonequilibrium discharges for combustion enhancement, such as dielectric barrier discharges (DBDs) and ultrashort-pulsed repetitive discharges (USRDs). Numerous studies [21–34] have reported stability enhancement in premixed flames, typically with extended flammability limits and reduced ignition delay times. With nonequilibrium discharges, only a small amount (0.1–1%) in comparison to the fuel energy content is added electrically to the combustible mixture, making the use of such plasma enhancement methods very practical. This is contrasted with the added energy of typical hydrogen pilot flames (1–5% of fuel energy content). Corresponding studies on the stability of diffusion flames are relatively rare. Kim et al. [35] found that a lifted methane jet flame in coflow is stable under application of a USRD in coflow velocities of up to 20 times the laminar flame speed, S_L . This enhancement corresponds to approximately 10 times the maximum natural coflow velocity ($2S_L$). Other plasma stabilization methods, such as dielectric barrier discharges ($3S_L$ of coflow velocity) and corona discharges ($2.5S_L$ of coflow velocity), were not as effective. Criner et al. [36] showed that the liftoff height of propane and air-diluted propane jet flames is reduced by more than 50% in the presence of a DBD. Leonov et al. [37] observed that a quasi-dc plasma can ignite and partially hold hydrogen and ethylene jet flames in a supersonic air flow. Klimov et al. [38] used combined dc/pulsed discharges to stabilize a propane diffusion flame in a vortex burner. Unlike premixed flames, the study of plasma-assisted diffusion flames is further complicated by the findings that the position of the discharge relative to the fuel jet is an additional critical factor in enhancing flame stability. Even for a relatively simple flame configuration such as a fuel jet in air coflow, the spatially nonuniform velocity and mixture fraction fields require carefully selected discharge electrode positions [35] for improved flame stability.

In the current study, we investigate USRD enhancement of flame stability in a more complex diffusion flame configuration—namely that of a methane

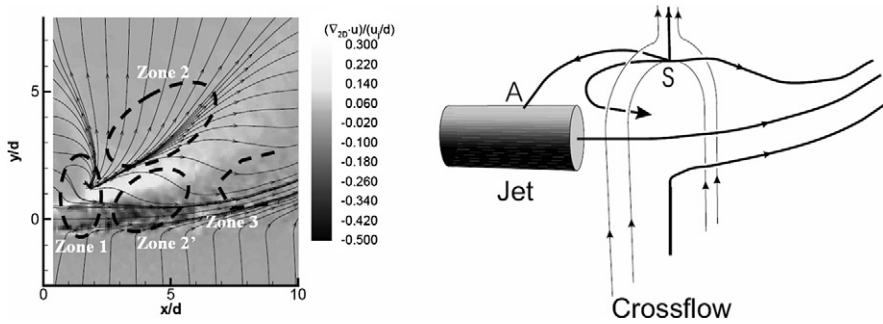


Fig. 1. Near-field stream traces and two-dimensional divergence determined from PIV from Hasselbrink and Mungal [39] for $R = 10$. Left: Two-dimensional divergence, overlaid with two-dimensional stream traces, in the near field. Zones 1, 2, 2', and 3 depict the main regions of interest in the current study. Right: Interpretation of three-dimensional near-field streamlines showing lee side saddle point.

jet in cross flow (JICF). The JICF has many practical applications, and the complexity of this flow configuration is highlighted in Fig. 1, taken from the results from Hasselbrink and Mungal [39]. Fig. 1 depicts the near-field time-averaged streamlines derived from PIV measurements (left panel), revealing the presence of flow recirculation in the wake and a leeward saddle point (see right panel). Areas of high 2-D divergence measured on the leeward side of the jet indicate a highly compressive out-of-plane strain, implying opposing out-of-plane streamlines that meet at the stagnation point, S . However, the near-zero 2-D divergence on the windward side implies that streamlines do not diverge strongly out of plane on the windward side; instead, they are entrained into the jet. Given this flow pattern, our efforts have focused on (i) finding optimal positions where electrodes should be placed to maximize the flame stability and (ii) determining the necessary mixture fraction for ignition that those positions share. Numerous scans of electrode placement along three independent directions are conducted to find the individual optimal positions in the near field of the JICF. The most interesting regions of the scans are denoted in Fig. 1 as Zone 1 (potential core, including the stagnation point S), Zones 2 and 2' (leeward and windward sides of the relatively upstream part of the near field, respectively), and Zone 3 (windward side of the relatively downstream part of the near field). Planar laser-induced fluorescence (PLIF) images of CH complement these data, as a preliminary attempt to investigate the role played by the discharge in affecting the initial ignition flame kernel.

2. Experimental setup

A schematic diagram of the experimental setup is provided in Fig. 2. A 30×30 cm square-cross-section wind tunnel with 80-cm-height test section produces

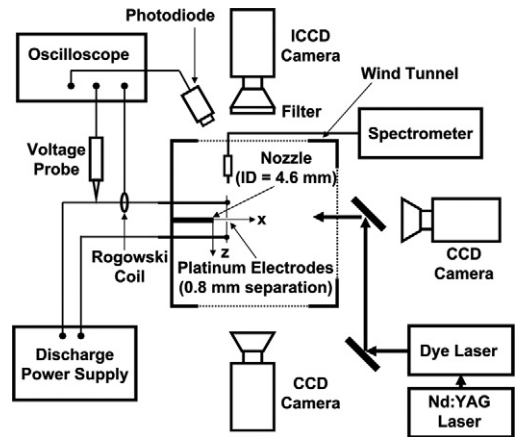


Fig. 2. Schematic of the experimental setup.

up to 7.7 m/s cross flow. The flow direction is out of the page as drawn. A methane jet is injected into the test section of the wind tunnel through a nozzle (4.6-mm inner and 6.4-mm outer diameter) perpendicular to the cross flow. In this study, the directions of nozzle and cross flow are denoted as x and y , respectively. The nozzle tip protrudes 10 cm from the sidewall of the wind tunnel 15 cm downstream from the test section inlet. In most of the experiments conducted in the current study, the speed of the jet varies from 8 to 51 m/s, so that the Reynolds number of the jet, Re_d , was between 2300 and 14,400. The cross-flow speed ranged from 0.6 to 7.7 m/s.

The USRD is produced by a pulse generator (FID Technology, Model SU-12). The peak voltage, repetition rate, peak current, and pulse width are typically 6 kV, 15 kHz, 15 A, and 15 ns (FWHM), respectively. The voltage and current pulse shapes are recorded by a 1000:1 high-voltage probe (Tektronics, Model P6015A) and Rogowski coil (Pearson Electronics, Model 2877), respectively, acquired simultaneously on a high-speed digital oscilloscope (Tek-

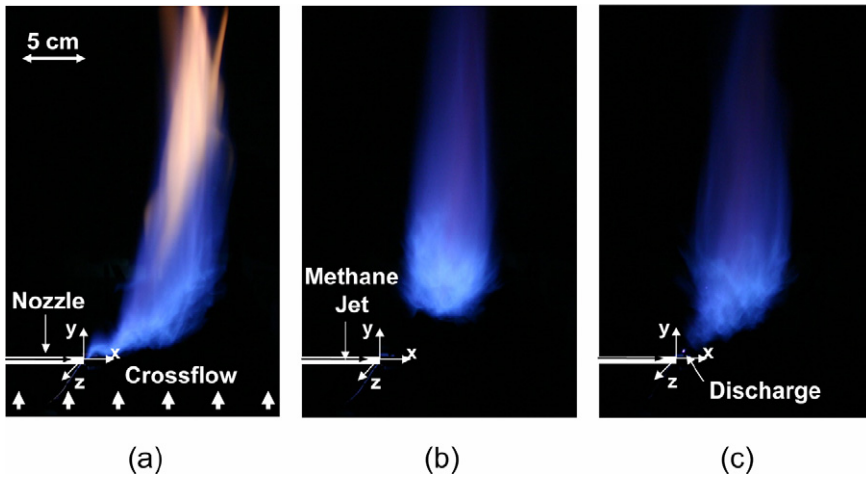


Fig. 3. Three photographs of the jet in cross flow. (a) Nozzle attached. $u_j = 8$ m/s ($Re_d = 2300$, where nozzle diameter d is 4.6 mm), $u_\infty = 0.6$ m/s, $R \sim 10$. (b) Lifted jet. $u_j = 14$ m/s ($Re_d = 4000$), $u_\infty = 1.5$ m/s, $R \sim 7$. (c) USRD attached jet. Flow conditions are identical to (b). Discharge has 6-kV peak voltage and 15-kHz repetition rate in case (c). The orientation of the 0.5-mm-diameter, 0.8-mm-separation platinum electrodes is parallel to the z direction. The discharge locations is $x/d = y/d = 3$ on a plane $z = 0$. The exposure time is $1/20$ s for every picture shown.

tronics, Model TDS 7104). A pair of opposed platinum (Pt) electrodes (0.5-mm diameter, 0.8-mm separation) is used for generating the USRD. The electrodes are oriented so that they are parallel to the z direction, i.e., perpendicular to the x and y coordinates, to minimize any possible interference with the flow. The positioning of the electrodes along the three independent coordinates, x , y , and z , are facilitated by three translational stages with micrometer precision and the positions are confirmed by images obtained from two interlaced CCD cameras (Kodak, ES 1.0) placed parallel to the x and z axes, respectively. A survey of the USRD emission spectra is also conducted in this study. The emission signal is transferred via a UV fiber optical cable and recorded by an optical spectrometer (Ocean Optics S2000) with 0.17-nm spectral resolution.

A fast-response (~ 10 ns) photodiode is used to detect the flame's broadband emission and to qualitatively confirm the presence of a flame, from which its duty cycle (defined as the fraction of the total time that the flame is ignited) is estimated. The total acquisition time to establish the duty cycle is 40 s for each electrode placement. The photodiode is positioned $\sim 100d$ (46 cm) and $20d$ downstream from the nozzle along the cross-flow and initial jet directions, respectively, and its field of view is approximately a $100d$ -diameter circular region. This measurement of the flame duty cycle at this downstream location averages out local flame fluctuations, which are known to occur at the downstream end of the flame [40]. The duty cycle reflects the residence time of large-scale self-sustaining

flames—an important measure of a flame's existence in a practical sense.

CH PLIF is performed using a 60 mJ/pulse laser sheet produced by a Nd:YAG (Spectra Physics Pro 290) pumped dye laser (Sirah Precision Scan) tuned to 390.23 nm. An Exalite 389/398 dye mixture is used to generate the desired wavelength. The resulting fluorescence is detected by an ICCD camera (Princeton Instruments PI-MAX) with a combination of 3-mm-thick KV-418 and BG-3 Schott glass filters. The detection wavelength is near 430 nm [3]. For the measurements reported here, the camera is triggered at 3 Hz with a 75-ns gate width.

As was done previously in our study of jet flames in coflow [35], a premixed flame of known equivalence ratio is used to calibrate the optical emission data obtained from the discharge kernel in the jet in cross flow, from which the local methane/air mixture fraction can be determined. The premixed flame is generated by a 44-mm-diameter swirl-stabilized mesoscale 6×6 array burner. A detailed description of the burner is given by Lee [41].

3. Results and discussion

3.1. Preliminary observations

Photographs of an attached burning JICF, a lifted burning JICF without the USRD, and a lifted burning JICF with the USRD are shown in Fig. 3 for comparison. In all cases, the camera exposure time is $1/20$ s. The x , y , and z coordinates, as defined in the previous section, are also shown in the figures, with the

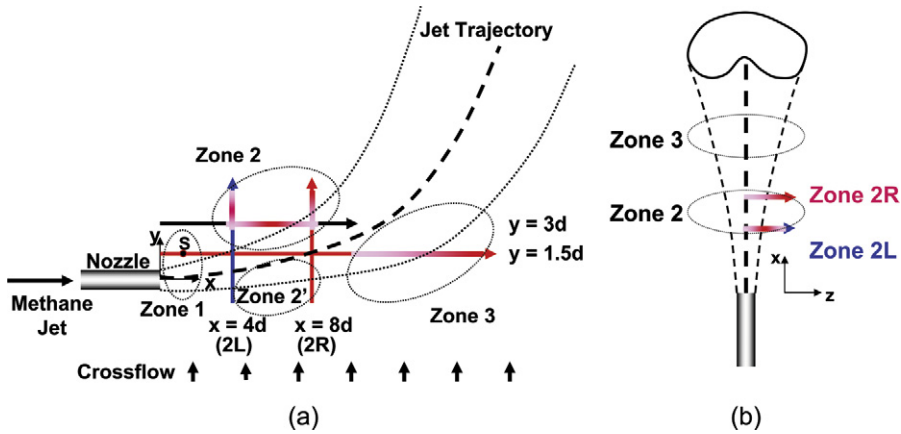


Fig. 4. Schematic of the geometric discharge scan along (a) x and y and (b) z axes. The solid lines represent the scanning directions. The thick and thin dotted lines correspond to the jet trajectories and the physical jet boundaries, respectively. The color-coded bands defined by Zones 1 to 3 represent regions that have nonzero duty cycle. The red color means a higher duty cycle while the pink color implies a lower duty cycle.

origin located at the center of the nozzle exit. For the photograph shown in Fig. 3a, the jet and cross-flow speeds are 8 m/s ($Re_d = 2300$) and 0.6 m/s, respectively, so that the square root of the momentum ratio $R = \sqrt{(\rho_j u_j^2)/(\rho_\infty u_\infty^2)} \sim 10$, with ρ representing the density, u the speed, and the subscripts j and ∞ the jet and cross-flow conditions, respectively. Apparent in Fig. 3a are two important features. First, the flame in the vicinity of the nozzle at the windward side experiences liftoff or local extinction away from the jet nozzle. This is also true even with use of a hydrogen pilot flame [42] at higher flow speeds. It is believed that the flame extinction in the vicinity of the windward region is mainly due to the high strain rate caused by the cross flow (see Fig. 1). Second, the flow patterns between upstream and downstream regions have clear differences. The upstream (near-field) trajectory is similar to that of an axisymmetric free jet, while the flow downstream (far-field) is affected by the recirculation effect of the cross flow (see Fig. 1). Finally, although it is not clearly seen from the picture, it is also known that the most upstream region ($1d$ – $2d$ from the nozzle [43]) of the near field forms the potential core of the jet.

With increasing jet and cross-flow speeds (and without the USRD again), the partially attached jet is lifted off as shown in Fig. 3b. In this particular case, the jet and cross-flow speeds are 14 m/s ($Re_d = 4000$) and 1.5 m/s, respectively, so that R is ~ 7 . It is noteworthy that the lifted flame eventually experiences blowout when the cross-flow speed is higher than ~ 2 m/s for this jet speed at normal injection. In the presence of a 6-kV-peak-voltage, 15-kHz-repetition-rate USRD, as shown in Fig. 3c (all flow conditions identical to those of Fig. 3b), the flame

base is pulled back to the vicinity of the discharge, which, for this case, is located at $x = 3d$ and $y = 3d$ on the $z = 0$ plane. The observation that the flame base is stabilized at a more upstream region that has higher flow speed in comparison to the no-discharge case (Fig. 3b) preliminarily confirms the significant effect of the discharge on enhancing flame stability.

As mentioned earlier, we observed that the stability enhancement of flames is an extremely sensitive function of discharge placement. Therefore, a more comprehensive survey of the response of the flame to discharge placement will be provided in the next section.

3.2. Observations of discharge scanning along the x , y , and z directions

To survey the effect of discharge placement on the flame duty cycle, we selected a total of nine scanning lines along directions parallel to the x , y , or z coordinates in the region of the near field. Five of these lines were along the y direction, with two lines each along the x and z directions. Throughout this scanning, the cross-flow speed (7.7 m/s), jet speed (51 m/s, $Re_d = 14,400$), and hence R (~ 5) are kept constant. It is noteworthy that no flame can be sustained under these flow conditions without the presence of the USRD. For this survey, the peak voltage and the repetition rate the discharge are also held at 6 kV and 15 kHz, respectively.

For purposes of discussion of the results, a schematic illustration of the side view and top view of the JICF is depicted in Figs. 4a and 4b, respectively. The thick dashed line represents the centerline trajectory, while the thin dotted lines correspond to the jet boundaries. The jet boundaries are sketched qualita-

tively based upon a preliminary visualization, using Mie scattering, of jet-seeded alumina particles illuminated by the second harmonic (532 nm) of a Nd:YAG laser. The scanning lines are shown as solid (black or colored) bands in the figure. Zones 1, 2, 2', and 3, defined in Fig. 1, are depicted as elliptical regions in the figures. While the detailed scanning geometry will be described later, it is noted that the color bands in Zones 2 and 3 correspond to the discharge locations which have nonzero duty cycle. For each band, strong red represents a relatively high duty cycle in comparison with the neighborhood, while a pink color corresponds to a relatively low duty cycle.

To investigate the flame duty cycle in the Zone 1, the placement of the electrode is varied along the lines $x = 1d$, $1.5d$, and $2d$ on a plane $z = 0$. Throughout the entire scanning in this zone, no flame ignition (that is, zero duty cycle) is observed for the discharge condition in the current study. As shown in the previous study for conventional JICFs [42], the zero duty cycle of the windward side in this region may be expected from the fact that the region has a significant strain rate that promotes local flame extinction. Conceivably, a high concentration fluctuation and a significant concentration gradient in this region can also affect the local extinction (more detailed investigations on the strain rate and scalar fields of the JICF will be discussed later). It is also noteworthy that the USRD placed in this zone shows a highly unstable characteristic resulting in an intermittent extinction of the discharge itself under these discharge conditions (6 kV and 15 kHz repetition rate). We believe this extinction is caused by the relatively large electron–methane inelastic collision cross section, resulting in a lower electron drift velocity and the interruption of the breakdown process.

The lack of flame ignition on the leeward side of Zone 1 may also be attributed to the vastly different flow and concentration patterns compared to the windward side, due to the presence of the saddle point, S . Based on the results of Su and Mungal [44] under similar flow conditions ($R \sim 5.7$), the saddle point is expected to be at $x = y = 1.5d$. As mentioned earlier, the neighborhood of this singular point has strong out-of-plane strain. We believe that the high degree of out-of-plane strain near S interferes with adequate mixing between fuel and air along the y direction. This poor mixing consequently hinders the propagation of a sustainable flame.

Duty cycle scans along a line $x = 4d$, $x = 8d$, and $y = 3d$ in a plane $z = 0$ are provided in Fig. 5a, as blue (triangle), red (square), and black (diamond) curves, respectively. The scan ranges are $-1d$ to $5d$ along the y direction and $1.5d$ to $10d$ along the x direction, spanning the zones 2 and 2'. Unlike the scans covering the potential core, the result shows that

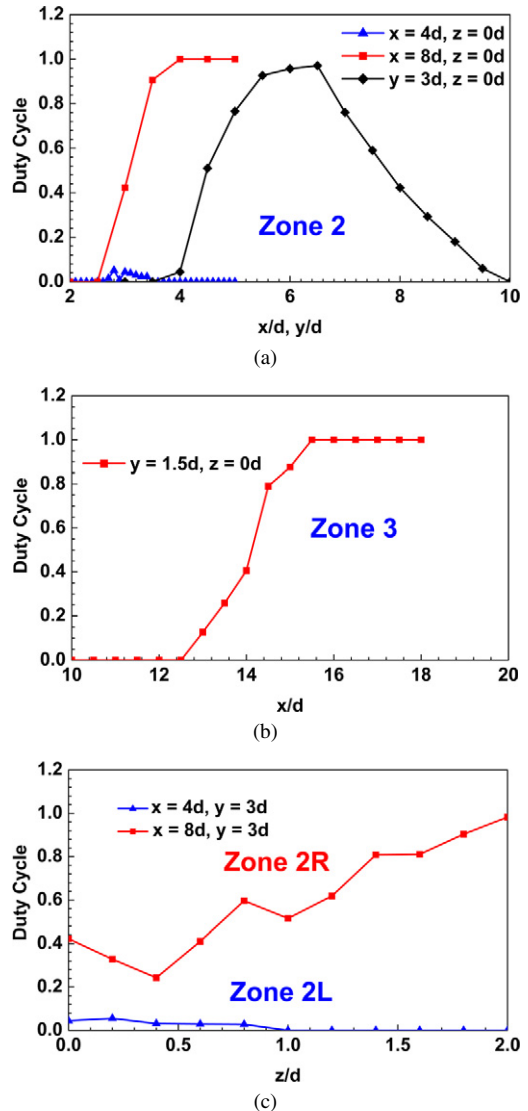


Fig. 5. Duty cycles as a function of discharge locations (a) in Zone 2, (b) in Zone 3, and (c) along the z direction. Flow conditions are $u_j = 51$ m/s ($Re_d = 14,400$), $u_\infty = 7.7$ m/s, $R \sim 5$, while discharge conditions are 6-kV peak voltage and 15-kHz repetition rate. Physical locations of Zones 2 and 3 are illustrated in Fig. 4.

there exists a significant variation in the duty cycle between the windward (zero duty cycle in Zone 2') and leeward (nonzero duty cycle in Zone 2) sides. We attribute the low duty cycle on the windward side to the presence of a significant strain rate, concentration fluctuation, and a high concentration gradient—characteristics that are expected to be less significant on the leeward side, resulting in a nonzero duty cycle in that region. More specifically, comparing scans along the $x = 4d$ and $x = 8d$ lines, we find low (but

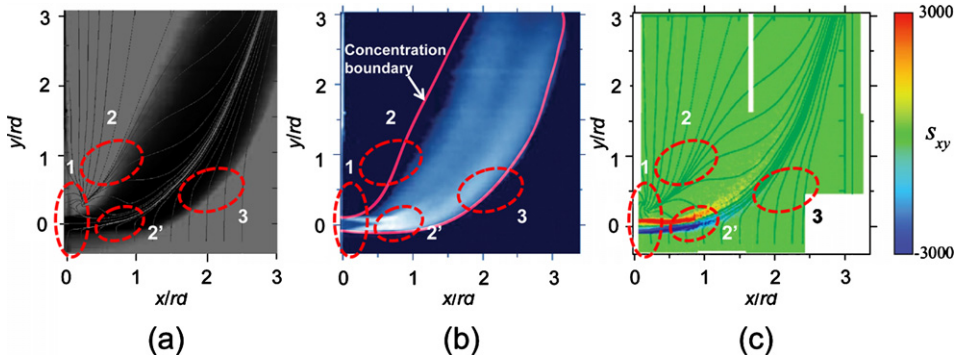


Fig. 6. Scalar and vector fields of acetone-seeded nitrogen-in-air cross flow [44]. (a) Concentration field overlaid with stream traces. Darker region represents higher jet concentration. The red dotted ellipses depict regions of interest. (b) Concentration fluctuation field. Red solid line represents a 1% concentration boundary. (c) Strain rate field overlaid with stream traces. For all figures, R is 5.7.

nonzero) duty cycles ($\sim 0.03 \pm 0.02$) along the former, and high duty cycles (up to unity) along the later line. This high duty cycle is also reached for scans line $y = 3d$ ($x = 4d$ to $x = 6.5d$). The decrease in duty cycle beyond $x = 6.5d$ is attributed to the placement of the electrode in an excessively fuel-rich region.

Despite seemingly adverse conditions, flame ignition and stabilization are sometimes possible with electrode placement on the windward side of the JICF. This is illustrated in Fig. 5b, for a scan along the x direction with $y = 1.5d$ and $z = 0$. Here we find a relatively wide plateau with unity duty cycle for $x > 15.5d$ (Zone 3 in Fig. 4). In this region, the strain rate in the velocity field is now diminished, and the concentration gradient is alleviated by the augmented mixing with the cross flow of air.

Fig. 5c presents scans of electrode positioning along the z direction for $x = 4d$ (triangles) and $x = 8d$ (squares) with $y = 3d$. The results are consistent with the scans of Fig. 5b, i.e., (i) the duty cycle for scans with $x = 4d$ is very low (~ 0.02) as the electrodes cross regions of the flow where there are significant adverse flow conditions, and (ii) the duty cycle for scans with $x = 8d$ is somewhat modest, generally increasing with increased values of z . It is noteworthy that in this more downstream location, there is more intermittency in the duty cycle, which we associate with local fluctuations associated with the presence of a large scale vortex structure. At a position of $y = 3d$, the discharge traverses a counterrotating vortex pair common to the JICF (see Fig. 4b). Within this counterrotating vortex pair, the discharge encounters intermittency in the instantaneous scalar field [43,44].

The scans of the electrode placement and resulting flame duty cycle suggest that factors that diminish the effectiveness of the discharge on igniting and stabilizing the flame include (i) gradients in the scalar concentration field; (ii) fluctuations in the scalar field; and

(iii) significant strain in the velocity field. To further assist in understanding the role played by these flow properties, the locations of the scanned Zones 1–3 are superimposed onto 2-D images of these properties and stream traces for an acetone-seeded nitrogen jet in air cross flow with $R = 5.7$ in Fig. 6 [44]. In Fig. 6a, the gray scale represents concentration (darker being higher). In Fig. 6b the color intensity represents a higher concentration fluctuation (white intensity being higher). The solid red line represents the jet concentration contour (1% of the initial jet concentration). The strain field is given by the color map in Fig. 6c, with red and blue corresponding to regions of high strain in the velocity field.

Zone 1 is characterized by abrupt changes in fuel/air concentration along the y direction. Here, the potentially flammable regions are quite thin, spanning a distance smaller than the scale of the discharge. Concentration fluctuations and in-plane strain rates are also very high on both the leeward and windward side, promoting local flame extinction. Again, no flame ignition is achieved by electrode placement in this zone. In Zone 2, mixing on the leeward side is more developed and the jet concentration gradient is weaker. Throughout this zone, concentration fluctuations and strain rates are low, and electrode placement in this zone results in improved flame stability. In contrast, the concentration gradient on the windward side across this region of the jet (Zone 2') is still relatively high, and the scalar fluctuation and strain rates are also high. As a result, unlike Zone 2, placement of the electrode in Zone 2' does not result in improved flame stability. Finally, in Zone 3, although concentration gradients are still relatively strong, fluctuations are reduced and the strain rate is completely relaxed. Electrode placement in this region results in improved flame ignition and stabilization. In this study, it may be noteworthy that we cannot explicitly point out

what is the most dominant factor that determines flame stability. Rather, we would like to emphasize how the complex scalar/velocity fields qualitatively affect the flame stability of the plasma assisted JICF. Detailed quantitative effects of the scalar/velocity fields will be the subject of future studies.

3.3. Mixture fraction at optimal discharge locations

In the previous section, we show that the improved duty cycle depends partly on the characteristics of the concentration field—i.e., the local ratio of air/fuel, or fuel mixture fraction. The measurement of instantaneous mixture fraction in a turbulent flame is still a challenging problem in experimental combustion studies. Various nonintrusive methods have been used to characterize mixture fractions, including Rayleigh/Raman scattering, Fourier transform infrared spectroscopy (FTIR), laser-induced fluorescence tunable diode laser absorption, laser-induced breakdown spectroscopy (LIBS), and spark spectroscopy. Many of these methods are difficult and costly to implement. In our studies, we employ a relatively novel method that is analogous to LIBS, but makes use of the spectral emission generated directly by the USRD. This method, which we refer to as plasma-induced breakdown spectroscopy (PIBS), has been described in more detail by Kim et al. [35] and is only briefly summarized here. In its implementation, simultaneous measurements of the flame duty cycle and the USRD emission spectra are recorded during the scanning of the electrodes. The intensity ratio of the 388-nm CN band to the 337-nm N₂ band is computed and compared to that observed from a USRD (at the same voltage and discharge frequency) placed in a fully premixed flame of known equivalence ratio, to establish the value of the mixture fraction in the jet flame in cross flow.

There are several reasons for the selection of the CN/N₂ ratio as the mapping function between the unknown local mixture fraction and the known equivalence ratio. In addition to being relatively intense and free of interferences, we find that the CN and N₂ bands increase and decrease monotonically, respectively, with increasing methane fraction over the range of the current study. Furthermore, the ratio of the two bands is found to be very sensitive to changes in mixture fraction.

The ratio is found to be a strong function of the peak discharge voltage and repetition rate [35], as shown in Fig. 7, where calibration curves of the CN/N₂ ratios vs the known equivalence ratio of a premixed methane/air flow are provided for a range of discharge voltage and repetition rate conditions. The PIBS results presented here correspond to conditions of 6-kV peak voltage and 15-kHz repetition rate (solid

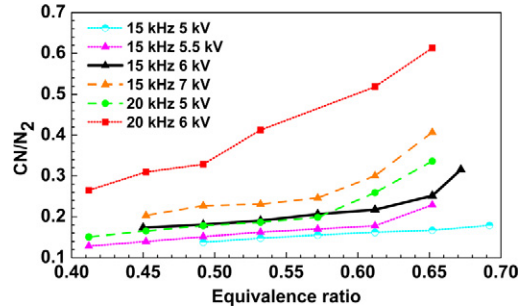


Fig. 7. Calibration curves of the CN/N₂ ratios vs the known equivalence ratio of a premixed methane/air flow for a range of discharge voltage and repetition rate conditions.

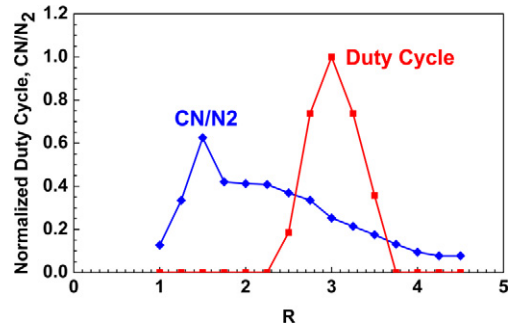


Fig. 8. A typical flame duty cycle normalized by its maximum value and the corresponding CN/N₂ ratio. Electrodes are located at $x/d = y/d = 3$ and $z = 0$. The discharge has 6-kV peak voltage and 15-kHz repetition rate. u_j varies in the range of 10–46 m/s ($2900 \leq Re_d \leq 13,000$) while u_∞ is fixed at 7.7 m/s.

line in Fig. 7). Based on our accuracy in measuring the fuel/air flow rates and the measured CN/N₂ intensity ratio, we estimate the accuracy in our assessment of the local mixture fraction to be ± 0.01 .

The duty cycle and corresponding CN/N₂ band intensity ratio at the electrode placement are investigated while varying R (i.e., varying jet speed with fixed cross-flow speed) as shown in Fig. 8. In this particular case, the electrode location is at $x = y = 3d$ and $z = 0$. The cross-flow speed is constant at a value of 7.7 m/s and the jet speed is varied between 10 and 46 m/s ($2900 \leq Re_d \leq 13,000$). Under these conditions, R sweeps the range 1–4.5. As shown, the electrode position is optimal at $R = 3$ and the corresponding CN/N₂ ratio is ~ 0.25 . This ratio is remarkably similar to that which we obtained using the same spectrometer (uncalibrated for relative spectral response) for the optimal electrode placement for a jet flame in coflow [35].

However, it is noteworthy that a value of 0.25 for the CN/N₂ ratio is in itself not a sufficient condition for flame ignition and stabilization, as it is apparent that there is another value of R (1.125) that results in

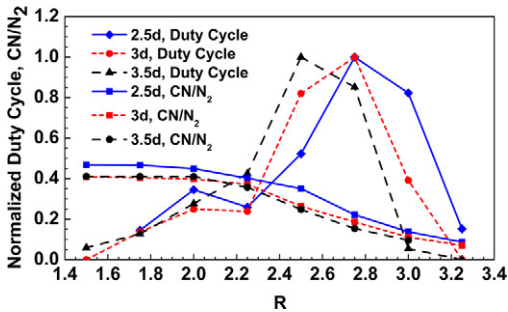


Fig. 9. Normalized duty cycle and corresponding CN/N_2 ratio as a function of R . The discharge and cross-flow conditions are identical to those in the previous cases (6 kV, 15 kHz, and 7.7 m/s). The range u_j is 18–33 m/s ($5000 \leq \text{Re}_d \leq 9400$). The x coordinate of the electrode position is fixed at $2.5d$ on a plane $z = 0$. The y coordinate are represented in the legend.

a similar CN/N_2 ratio at the electrode placement, but where the duty cycle is zero. Jet visualization using planar Mie scattering shows that the discharge placement for $R = 1.125$ corresponds to the windward side, at a region equivalent to Zone 2', characterized by strong gradients and fluctuations in concentration and a high strain field. In light of the analysis presented above, it is not surprising that the discharge is incapable of igniting the flame despite the value of R in this region. The abrupt change in mixture fraction is confirmed from the sharp increase in the CN/N_2 ratio in the range from $R = 1$ to $R = 1.5$.

Similar results are shown in Fig. 9, in this case, for variations in R , with the electrode placed at a position $x = 2.5d$, $z = 0$, and y varying from $2.5d$ to $3.5d$. The cross-flow speed is constant at 7.7 m/s, while the jet speeds are varying from 18 m/s ($\text{Re}_d \sim 5000$) to 33 m/s ($\text{Re}_d \sim 9400$), so that the corresponding R sweeps the range from 1.75 to 3.25. From the figure, it is seen that the optimal CN/N_2 ratios are essentially the same (0.22 ± 0.03) for all three cases, and comparable to that seen in Fig. 8 (~ 0.25) and in previous experiments with jet flames in coflow.

Through calibrations with the same discharge placed in premixed flames of known fuel/air mixture ratios, as shown in Fig. 7, the optimal CN/N_2 band intensity ratio of 0.22–0.25 is found to correspond to an equivalence ratio of 0.63–0.65. This mixture fraction is much leaner than a stoichiometric methane/air flame. Furthermore, it is noted that a conventional lifted methane jet flame is primarily stabilized near the stoichiometric mixture fraction [45]. We attribute this observed difference to three phenomenon: (i) the higher energy coupling to the flow in leaner regions, as we observe that there is no discharge when the electrode is placed in the jet core; (ii) the greater cross section for electron dissociation of methane, which

produces more radicals (e.g., H), which can subsequently react with molecular oxygen to produce OH, an important initiator of combustion; and (iii) inherent intermittency of the flow, whereby the discharge excites both instantaneous concentration regions and entrained air regions, which together compose the local mean mixture fraction. These conjectures would, however, require further investigations.

Finally, it is noteworthy that the optimal mixture fraction obtained here is only valid under the given discharge condition of the current study, 6-kV voltage and 15-kHz repetition rate. This is because nonlinear power coupling between the discharge and the premixed media causes different local concentrations of discharge-induced species with variation of the discharge conditions. The changes of the local concentrations tend to shift the optimal mixture fractions obtained in this study. While we speculate that the electron impact collision cross section of parent species and the electron energy distribution function, which vary with the reduced electric field, play a central role in the shift, more comprehensive investigation on this issue will be described in our future studies.

3.4. Preliminary observations of the discharge and flame kernel

We have shown above that the USRD increases the flame stability of the jet in cross flow. Its effect is strongest when the discharge is positioned at regions in the flow where the ratio of mixture fractions ($Z_{\text{OPT}}/Z_{\text{ST}}$) is in the range of ~ 0.63 – 0.65 . In this section, we seek to better understand the role played by the discharge in stabilizing the flame. It is possible that the USRD provides a direct means of igniting the flame, anchoring the flame base at the discharge kernel (within a length scale defined by the flow velocity and ignition delay time—typically ~ 1 mm). A consequence of this would be the repetitive ignition during the presence of the discharge and the subsequent lack of ignition during the absence of the discharge in one pulse cycle. Alternatively, it is possible that the pulsed discharge plasma is a source of long-lived radicals or stable species that influence flame ignition, with recombination times $> 100 \mu\text{s}$. In this case, a flame can be stabilized through accelerated chemical reactions by a nearly steady reactive flow generated by the discharge.

Planar LIF (PLIF) images of CH radicals (see Fig. 10) in the vicinity of the discharge and flame base reveal features that may guide us in establishing the mechanism for flame stabilization. The images in Fig. 10 are representative of the flame-base structure at random time samplings. The placement of the USRD is at $x/d = 3$ and $y/d = 3$, with $R = 3$ and jet $\text{Re}_d \sim 4000$ (jet velocity is 14 m/s). The peak voltage

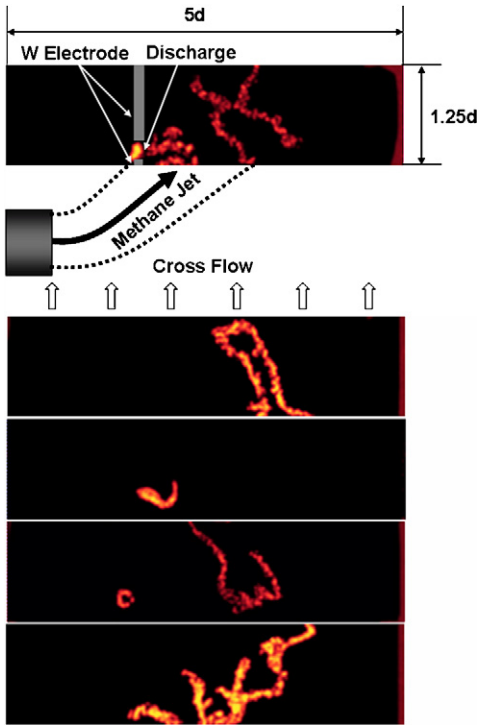


Fig. 10. Instantaneous CH PLIF images at a random time. The physical orientations of the jet, cross flow, and electrodes are represented in the first picture. Bright yellow spots represent CH radicals from discharge, while the randomly shaped curve illustrates CH radicals due to a flame. In the particular case, 0.8-mm separation and diameter blunt tungsten electrodes whose orientation is parallel to the y direction are placed at $x/d = y/d = 3$. The USRD has 6-kV peak voltage and 15-kHz repetition rate. Flow conditions are $u_j = 14$ m/s ($Re_d = 4000$), $u_\infty = 3.5$ m/s, so that R becomes ~ 3 .

and repetition rate are 6 kV and 15 kHz, respectively. For these studies the electrodes are oriented along the y axis and are fabricated from 0.8-mm-diameter tungsten. This electrode reorientation was necessary to facilitate the detection of discharge CH fluorescence, since the ICCD camera used for fluorescence detection is aligned along the z direction. The cross-flow speed was reduced to 3.5 m/s (compared to 7.7 m/s, used above) as the slower cross-flow speed resulted in a lower jet fluctuation, and a better chance at capturing CH PLIF images of the flame base in the field of view that included the discharge. In the figure, the discharge is represented as a bright yellow spot. The cross-flow direction is from the bottom to the top and the fuel jet is discharged from the bottom left to the right. During the image acquisition, the duty cycle of the downstream flame was unity.

The PLIF images indicate that the flame base appears to have a random spatial distribution similar

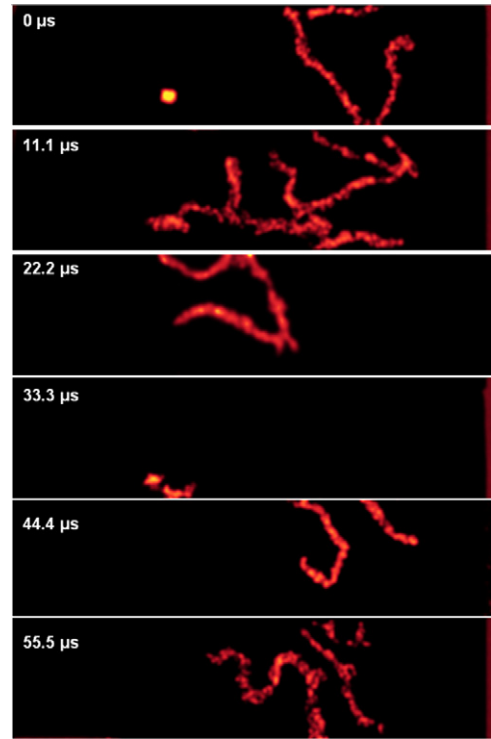


Fig. 11. Phase-locked CH PLIF images under conditions identical with Fig. 10. The bright spot at 0 μ s is the location of discharge for all images.

to what is seen in a conventional turbulent lifted jet in cross flow ($Re_d = 4000$) [46]. However, the more interesting observation is that there usually exists a noticeable separation (~ 1 cm) between the discharge kernel and the flame base. We conjecture that the flame does not experience direct ignition from the discharge and that the medium that fills the gap may play an important role in igniting and stabilizing the flame.

Results of phase-locked CH PLIF, which provides information about the temporal correlation between the USRD and the flame base, are illustrated in Fig. 11. These images are obtained under the same flow, discharge, and electrode conditions as those of Fig. 10. The six images shown are obtained by phase-shifting the laser within a single pulse cycle (15 kHz), i.e., in phase (0 μ s), 1/6 out of phase (11.1 μ s), 2/6 out of phase (22.2 μ s), etc. From these images, it can be concluded that there is no specific temporal correlation between the actual discharge and overall flame ignition. This finding is further confirmed statistically in Table 1. The table represents the number of images, out of 400 images in each case, in which the nearest distance between the flame and the discharge is less than ~ 1 mm (~ 10 m/s \times 100 μ s), the typical length scale of possible direct flame ignition from a discharge. Even in the case of in-phase (~ 0 μ s) trig-

Table 1

Number of images whose nearest flame branch is within 1 mm from the discharge

	0	11.1 μs	22.2 μs	33.3 μs	44.4 μs	55.5 μs
Number of images	65	59	60	61	60	64

Note. Total number of images is 400 in each case. 0 μs means in phase with the discharge firing. The experimental conditions are identical to those of Fig. 10.

gering, the number of flames (65) that are present in the vicinity of the discharge is not significantly different from that in the substantially out-of-phase cases, such as the 5/6 cycle phase-shift condition (64).

The finding that the ignition of the flame has little spatial and temporal correlation within the discharge ignition cycle imply that the USRD “induces” the ignition of the flame by producing a steady but active stream of species that assist in the flame ignition, rather than providing a direct and instantaneous ignition of the flame (e.g., by local heat release). Based on this finding, further questions arise, which include the identification, origin, and characteristics of the ignition stream and the structure of a plasma-enhanced flame. While the detailed description on these issues is beyond the scope of the current study, we summarize here the results we have obtained thus far [47]. The results draw attention to the possibility that there exists a low-temperature preoxidation stream from the discharge gap. This flow, which we call a “preflame,” is composed of intermediate species such as H_2 and CO as well as reactive radicals such as OH that originate from the excited N_2 and N in the discharge. The abundance of excited N_2 in the vicinity of the discharge and reactive OH in the preflame was confirmed by emission spectrum analysis in our previous study [32]. Also, the presence of intermediate species including H_2 and CO in the preflame and their central role in stabilizing premixed flames are observed in our currently on-going one-dimensional simulation using PREMIX and OPPDIF as well as initial radical yield calculation in the vicinity of the discharge. The preflame can be characterized by higher vibrational (reactive) and lower rotational temperatures (cold) in comparison to a conventional high-temperature flame [32]. We believe that the preflame can ignite the rest of the surrounding mixture to form conventional high-temperature flames. Therefore, the flame kernel has a multilayer structure that consists of both a cold preflame and a high-temperature main flame. A more detailed description, with supporting chemical kinetic simulations, will be provided in future studies.

4. Conclusions

A survey of physical locations of the optimal discharge placement and their common mixture fraction

was performed for a JICF. As a plasma discharge, highly nonequilibrium ultra-short-pulsed repetitive discharge (USRD) was used, while a methane jet in cross flow was the flame configuration in the current study. As a criterion to determine the optimal discharge placement, the flame duty cycle, defined by the fraction of the total time that the flame is ignited, was used. The physical scanning of the discharge location was carried out along the directions x (parallel to the initial jet direction), y (parallel to the cross flow direction), and z (direction perpendicular to the x and y coordinates). While it was found that the duty cycle is a strong function of the discharge location, we found that the flow characteristics, such as adequate jet concentration, low concentration gradient, low scalar fluctuation, and low strain rate, are the primary factors that determine the possibility of flame ignition. As summarized in Figs. 12a and 12b, Zone 1 (potential core of JICF) has an excessively high concentration and strain rate to be ignited. Also, the mixing in this region is not sufficiently developed to allow ignition; therefore, the concentration gradient is significantly high. The high fluctuation and strain rate are diminished further downstream (Zone 2, upstream and leeward parts of the near field). In addition, the concentration profile along the y direction in Zone 2 has relaxed so that the flame is ignitable in this region. Zone 2' (upstream and windward parts of the near field), however, is nonignitable due to the high concentration gradients, high concentration fluctuation, and excessive strain rate. Flame ignition in Zone 3 (downstream and windward parts of the near field) is possible due to its moderate concentration gradient and low strain rate. Along the z direction, the duty cycle shows significant fluctuations in comparison to the other two directions. This is caused by the complex vortex structure and intermittent scalar field in the scanned region.

A common mixture fraction that the optimal discharge positions have was determined by plasma-induced breakdown spectroscopy (PIBS). By detecting the ratio of the peak emission intensity of the 388-nm CN band to that of the 337-nm N_2 band, followed by calibration via an identical experiment in a premixed flame that has a known equivalence ratio, an optimal mixture fraction was obtained as $Z_{\text{OPT}}/Z_{\text{ST}} \sim 0.63\text{--}0.65$. The obtained value showed

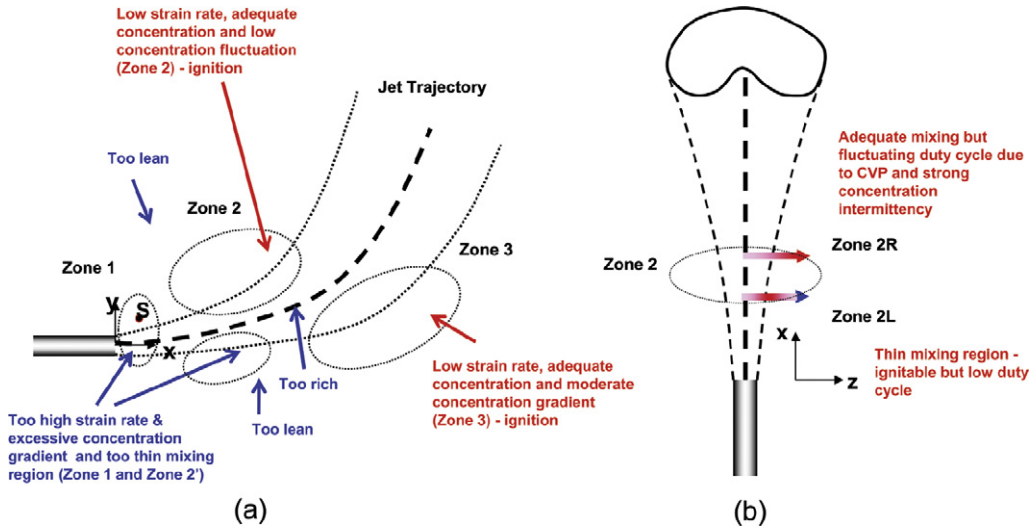


Fig. 12. Summary of duty cycle affecting scalar and flow factors.

that a plasma-assisted flame is stabilized in a leaner region than a conventional flame.

Finally, CH PLIF imaging was carried out to achieve a preliminary investigation on the role of a discharge in igniting a flame. Through the investigation of the spatial and temporal correlations between discharge and flame ignitions, it was concluded that there exists no strong correlation between the two. This finding implied that it is most likely that a discharge is a steady source of reactive species to increase the flame stability rather than an instantaneous ignition source of the flame. Our ongoing studies use this information to develop a model of plasma flame ignition that consists of a cold preflame followed by a high-temperature conventional flame [47].

Acknowledgments

This work is sponsored by the AFOSR/MURI Program—Experimental/Computational Studies of Combined-Cycle Propulsion: Physics and Transient Phenomena in Inlets and Scramjet Combustors, with Julian Tishkoff as the Technical Monitor. The authors express their gratitude to Professor L. Su for providing figures on scalar concentration, concentration fluctuation, and strain rate fields.

References

- [1] D. Han, M.G. Mungal, *Proc. Combust. Inst.* 28 (2001) 261–267.
- [2] L. Muñiz, M.G. Mungal, *Combust. Flame* 126 (1–2) (2001) 1402–1420.
- [3] C.D. Carter, J.M. Donbar, J.F. Driscoll, *Appl. Phys. B* 66 (1) (1998) 129–132.
- [4] S. Prakash, S. Nair, T.M. Muruganandam, Y. Neumeier, T. Lieuwen, J. Seitzman, B.T. Zinn, in: 43rd AIAA Aerospace Sciences Meeting and Exhibit, Reno, NV, 2005.
- [5] S. Tachibana, S. Zimmer, Y. Kurosawa, K. Suzuki, in: 2nd Asian Joint Conference on Propulsion and Power, Kitakyushu, Japan, 2005.
- [6] R.W. Schefer, M. Namazian, J. Kelly, *Combust. Sci. Technol.* 56 (4–6) (1987) 101–138.
- [7] D.T. Yegian, R.K. Cheng, *Combust. Sci. Technol.* 139 (1–6) (1998) 207–227.
- [8] S. Archer, A.K. Gupta, in: 2nd International Energy Conversion Engineering Conference, Providence, RI, 2004.
- [9] H.F. Calcote, *Proc. Combust. Inst.* 3 (1949) 245–253.
- [10] H.F. Calcote, R.N. Pease, *Ind. Eng. Chem.* 43 (1951) 2726–2731.
- [11] H.F. Calcote, C.H. Berman, in: Fossil Fuel Combustion Symposium, Houston, TX, 1989, p. 25.
- [12] M.L. Polanyi, G.H. Markstein, *Phenomena in Electrically and Acoustically Disturbed Flames*, Project SQUID Technical Report, Cornell Aeronautical Laboratory, 1947.
- [13] G.P. Tewari, J.R. Wilson, *Combust. Flame* 24 (1975) 159–167.
- [14] C.S. Maclatchy, R.M. Clements, P.R. Smy, *Combust. Flame* 45 (1982) 161–169.
- [15] J. Lawton, F.J. Weinberg, *Electrical Aspects of Combustion*, Oxford Univ. Press, London, 1969.
- [16] A.B. Fialkov, *Prog. Energy Combust. Sci.* 23 (1997) 399–528.
- [17] S.H. Won, M.S. Cha, C.S. Park, S.H. Chung, *Proc. Combust. Inst.* 31 (2007) 963–970.
- [18] F.J. Weinberg, K. Hom, A.K. Oppenheim, K. Teichman, *Nature* 272 (1978) 341–343.
- [19] F.B. Carleton, I.M. Vince, F.J. Weinberg, *Proc. Combust. Inst.* 19 (1983) 1523–1531.

- [20] A.J.J. Lee, F.J. Weinberg, *Nature* 311 (1984) 738–740.
- [21] S.A. Bozhenkov, S.M. Starikovskaia, A.Yu. Starikovskii, *Combust. Flame* 133 (2003) 133–146.
- [22] E.I. Mintousov, S.V. Pancheshnyi, A.Yu. Starikovskii, in: 42nd AIAA Aerospace Sciences Meeting and Exhibit, Reno, NV, 2004.
- [23] A.Yu. Starikovskii, *Proc. Combust. Inst.* 30 (2005) 2405–2417.
- [24] S.M. Starikovskaia, I.N. Kosareve, A.V. Krasnohub, E.I. Mintousov, A.Yu. Starikovskii, in: 43rd AIAA Aerospace Sciences Meeting and Exhibit, Reno, NV, 2005.
- [25] W. Kim, H. Do, M.G. Mungal, M.A. Cappelli, in: WSS/CI Fall Meeting, Stanford, CA, 2005.
- [26] N. Chintala, A. Bao, G. Lou, I.V. Adamovich, *Combust. Flame* 144 (2006) 744–756.
- [27] D. Galley, G. Pilla, D.A. Lacoste, S. Ducruix, F. Lacas, D. Veynante, C.O. Laux, in: 43rd AIAA Aerospace Sciences Meeting and Exhibit, Reno, NV, 2005.
- [28] S. Pancheshnyi, D. Lacoste, A. Bourdon, C.O. Laux, in: European Conference for Aerospace Sciences, Moscow, Russia, 2005.
- [29] G. Lou, A. Bao, M. Nishihara, S. Keshav, Y.G. Utkin, I.V. Adamovich, in: 44th AIAA Aerospace Sciences Meeting and Exhibit, Reno, NV, 2006.
- [30] E.I. Mintousov, A.A. Nikipelov, S.M. Starikovskaia, A.Yu. Starikovskii, in: 44th AIAA Aerospace Sciences Meeting and Exhibit, Reno, NV, 2006.
- [31] S.M. Starikovskaia, N.B. Anikin, I.N. Kosarev, N.A. Popov, A.Yu. Starikovskii, in: 44th AIAA Aerospace Sciences Meeting and Exhibit, Reno, NV, 2006.
- [32] W. Kim, H. Do, M.G. Mungal, M.A. Cappelli, *Proc. Combust. Inst.* 31 (2007) 3319–3326.
- [33] N.A. Popov, I.A. Kossyi, in: 45th AIAA Aerospace Sciences Meeting and Exhibit, Reno, NV, 2007.
- [34] E.I. Mintousov, E.Y. Svetlana, A.A. Nikipelov, S.S. Starikovskaia, A.Yu. Starikovskii, in: 45th AIAA Aerospace Sciences Meeting and Exhibit, Reno, NV, 2007.
- [35] W. Kim, H. Do, M.G. Mungal, M.A. Cappelli, *IEEE Trans. Plasma Sci.* 34 (2006) 2545–2551.
- [36] K. Criner, A. Cessou, J. Louiche, P. Vervisch, *Combust. Flame* 144 (2006) 422–425.
- [37] S.B. Leonov, A.Y. Dmitry, A.P. Napartovich, I.V. Kochetov, in: 44th AIAA Aerospace Sciences Meeting and Exhibit, Reno, NV, 2006.
- [38] A. Klimov, V. Bitiurin, I. Moralev, B. Tolkunov, K. Zhirnov, V. Kutlaliyev, A. Nikitin, A. Velichko, I. Biler, in: 45th AIAA Aerospace Sciences Meeting and Exhibit, Reno, NV, 2007.
- [39] E.F. Hasselbrink Jr., M.G. Mungal, *J. Fluid Mech.* 443 (2001) 27–68.
- [40] M.G. Mungal, A. Lozano, *Exp. Fluids* 21 (1996) 264–267.
- [41] S. Lee, C.F. Edwards, C.T. Bowman, in: ASME Int. M.E. Congress and RD&D Expo, Anaheim, CA, 2004.
- [42] E.F. Hasselbrink, M.G. Mungal, *Proc. Combust. Inst.* 27 (1999) 1167–1173.
- [43] S.H. Smith, M.G. Mungal, *J. Fluid Mech.* 357 (1998) 83–122.
- [44] L.K. Su, M.G. Mungal, *J. Fluid Mech.* 513 (2004) 1–45.
- [45] A. Joedicke, N. Peters, M. Mansour, *Proc. Combust. Inst.* 30 (2005) 901–909.
- [46] D. Han, M.G. Mungal, *Proc. Combust. Inst.* 29 (2003) 1889–1995.
- [47] W. Kim, M.G. Mungal, M.A. Cappelli, *Appl. Phys. Lett.* 92 (2008) 051503.